Heliyon 9 (2023) e20107

Contents lists available at ScienceDirect

Heliyon

journal homepage: www.cell.com/heliyon

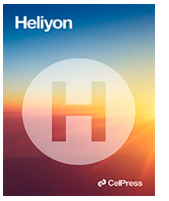

Investigation of the treatment potential of Raloxifene-loaded polymeric nanoparticles in osteoporosis: In-vitro and in-vivo analyses

Zhonghua Guo [a], Rabia Afza [b], Muhammad Moneeb Khan [c,d], Saif Ullah Khan [e,**], Muhammad Waseem Khan [f], Zakir Ali [c,d], Sibgha Batool [c,d], Fakhar ud Din [c,d,*]

[a] Department of Orthopaedics, Henan Province Hospital of TCM, Zhengzhou City, Henan Province, 450002, China
[b] Department of Botany, Hazara University Mansehra KP, Pakistan
[c] Department of Pharmacy Quaid-i-Azam University, 45320, Islamabad, Pakistan
[d] Nanomedicine Research Group, Department of Pharmacy Quaid-i-Azam University, 45320, Islamabad, Pakistan
[e] Institute of Biotechnology and Microbiology, Bacha Khan University, Charsada, KPK, Pakistan
[f] Institute of Pharmaceutical Sciences Khyber Medical University, Peshawar, Pakistan

ARTICLE INFO

Keywords:
Osteoporosis
Raloxifene, polymeric nanoparticles
Bioavailability
Oral administration

ABSTRACT

Osteoporosis (OP), is a systemic bone disorder associated with low bone mass and bone tissue corrosion. Worsening of the disease condition leads to bone delicacy and fracture. Various drugs are available for the treatment of OP, however they have limitations including poor solubility, bioavailability and toxicity. Herein, Raloxifene-loaded polymeric nanoparticles (RLX-PNPs) were developed and investigated for the treatment of OP with possible solutions to the above mentioned problems. RLX-PNPs were prepared by modified ionic gelation method followed by determining their particle properties. FTIR, DSC and PXRD analysis of the RLX-PNPs were performed to check chemical interaction, thermal behavior and crystallinity, respectively. In-vitro release profile of RLX-PNPs was checked in lab setting, whereas its pharmacokinetics was investigated in Sprague-Dawley rats, in-vivo. Finally, the treatment potential of RLX-PNPs was analyzed in OP induced animal model. The optimized PNPs formulation indicated 134.5 nm particle size, +24.4 mV charge and 91.73% % EE. TEM analysis showed spherical and uniform sized particles with no interactions observed in FTIR analysis. In-vitro release of RLX from RLX-PNPs showed more sustained release behavior as compared to RLX-suspension. Moreover, pharmacokinetic investigations showed a significantly enhanced bioavailability of the RLX-PNPs as well as reduced serum levels of alkaline phosphatase and calcium in OP induced rats when compared with RLX-Suspension after oral administration. Findings of this study suggested that the developed RLX-PNPs have the potential to treat OP due to sustained release and improved bioavailability of the incorporated drug.

* Corresponding author. Department of Pharmacy Quaid-i-Azam University, 45320, Islamabad, Pakistan.
** Corresponding author.
E-mail addresses: saifullahkhan@bkuc.edu.pk (S.U. Khan), fudin@qau.edu.pk (F. Din).

https://doi.org/10.1016/j.heliyon.2023.e20107
Received 13 February 2023; Received in revised form 23 August 2023; Accepted 12 September 2023
Available online 13 September 2023

1. Introduction

Osteoporosis (OP) is a bone disease associated with thinning of bone masses and bone tissue deterioration which ultimately leads to increased susceptibility towards bone fragility and bone fracture particularly of the hip, wrist and spine [1]. OP usually occurs in old age individuals, associated with increased tendency of fragility and breakage as a result of reduced bone density [2]. Progression of OP occurs without any evident signs until a fracture happen, so it is referred as "silent disease" [3]. Globally, it is projected to affect over 200 million people worldwide [4]. It is also estimated that the number of hip fractures cases may rise to 6.26 million by the year 2050 [5,6]. A number of drugs are in use for treating OP, including alendronate, raloxifene, zoledronic acid and risedronate [3,7]. These drugs serve as potential treatment options against a number of post-menopausal situations in women and osteosis in both genders. Similarly, other agents like simvastatin [8] and teriparatide [9] are also employed in the treatment of OP. Other therapeutic strategies include the use of bisphosphonates to treat bone degradation associated with OP by increasing bone mass, strength and turnover.

In 1997, United State food and drug administration (FDA) approved the use of Raloxifene HCl (RLX) in the treatment of OP. It is one of the safest drugs used for the prevention and treatment of OP, when used for long term [10]. Mechanism of RLX in OP is shown in (Fig. 1). RLX is available in oral dosage form, however is faced with some potential limitations like extensive first-pass effect, inadequate absorption and low bioavailability [11]. These challenges have minimized the therapeutic utilization of RLX, so there is a dire need for better and effective dosage forms to enhance its clinical efficacy in OP patients. One such approach could be the fabrication of polymeric nanoparticles (PNPs). PNPs are the particulate nano-carriers used extensively in biomedicine due to their promising attributes in drug delivery, such as sustained and controlled release drug profile, nano-ranged size and biocompatibility [12]. They are further classified into nanospheres and nanocapsules [13]. Over the past two decades, various polymers have been utilized in the preparation of PNPs [14]. Some of those polymers includes, Chitosan (CTX) [15], Eudragit S100 [16], Hydroxyl propyl methyl cellulose [17],Poly lactic co-glycolic acid [18], Pluronic polymer [19] and Chondroitin sulfate [20], that have been extensively utilized for the preparation of PNPs. Among these CTX has excellent polymeric properties including its biocompatible and biodegradable nature [21]. CTX is vastly employed in the field of nanomedicine based on its numerous applications including muco-adhesive nature, poly-anionic cross linking and avoids the use of toxic solvents [22].

The present work was designed to develop and evaluate potential of polymeric nanoparticles loaded with raloxifene (RLX-PNPs) as a carrier with sustained release, improved pharmacokinetic and therapeutically augmented anti-osteoporotic effects. Novelty of the research work is that the RLX incorporated polymeric nanoparticles has never been reported so far to the best of our knowledge and available literature. Moreover, it is for the very first time that RLX-PNPs are prepared with enhanced therapeutic potential in the OP induced animal model.

2. Experimental section

2.1. Materials

Raloxifene (RLX), Chitosan (CTX) and Sodium tripolyphosphate (STPP) were bought from Sigma Aldrich, Germany. Dialysing

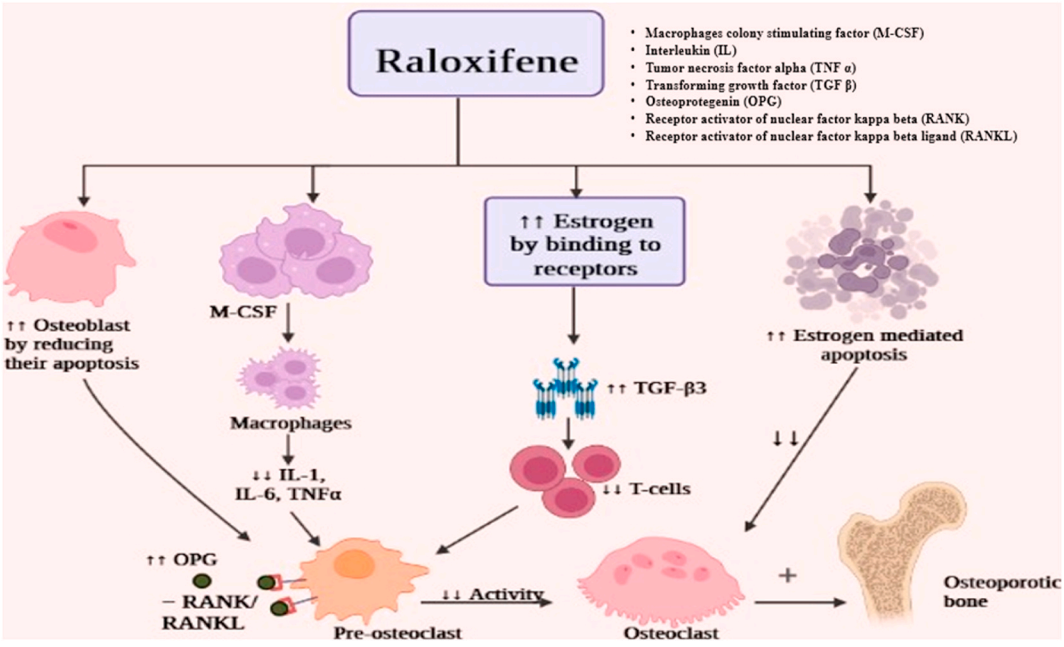

Fig. 1. Illustration of the mechanism of raloxifene in the treatment to of osteoporosis.

membrane was purchased from Spectrum Laboratories, Inc. (Los Angeles, CA USA). Potassium dihydrogen phosphate, Potassium chloride, Disodium hydrogen and Sodium chloride phosphate were bought from Merck, Karachi Pakistan. Tween®80, were kindly gifted by Biolabs Islamabad, Pakistan. All other chemicals were pure compounds obtained from local market, Islamabad Pakistan.

3. Methods

3.1. Preparation of RLX-PNPs

PNPs were prepared with ionic gelation method as reported earlier [23]. Momentarily, CTX solutions (in 1% acetic acid solution) were prepared via overnight magnetic stirring. At the same time, STPP solutions (in deionized water) were prepared using constant magnetic stirring. Later on, 5 ml CTX solution was mixed with Tween®80 under continuous magnetic stirring at 1600 rpm for 3 h, followed by the addition of RLX. At this stage, STPP solution (2 ml) was added portion wise and was kept at 700 rpm for 1 h. Lastly, centrifugation of the mixture was done at 14000 rpm to for 3 h to obtain adequate pellets of RLX-PNPs [24,25].

4. Characterization of RLX-PNPs

4.1. Particle properties

Particle properties of the prepared RLX-PNPs were analyzed with Zeta sizer (ZS-90, Malvern instrument, UK), which was equipped with He–Ne laser. Machine was operated at room temperature at a wavelength of 635 nm and a static angle of 90°. Briefly, 10 μl of the prepared RLX-PNPs were diluted in 1 ml distilled water and were sonicated for 2 min followed by particle size and polydispersity index (PDI) analysis. Furthermore, the Universal dip cell was added into the sample, followed by the investigation of zeta potential. Graphs of all the samples were drawn using software [26].

4.1.1. Percent drug entrapment (%DE)

Indirect method was utilized to found the %DE of the RLX-PNPs [27,28]. Momentarily, 1 ml of RLX-PNPs were centrifuged at 13, 000 rpm for 12 min. Filtrate was diluted using acetonitrile followed by its HPLC (Kyoto, Japan) analysis for quantification of the free RLX. HPLC system was an auto sampler system fortified with C-18 column (150 mm × 4.6 mm, 5 μm) and SPD M20-AV detector. Deionized water and pure methanol at their respective values of 57:43 were used as mobile phase in the presence of 0.2% glacial acetic acid. Flow rate and injection volume of the mobile phase was set at 1.2 ml/min and 20 μl, respectively. Quantification of the drug was done at 287 nm wavelength [11]. RLX concentration was determined using the calibration curve followed by the determination of % DE using the following equation:

$$\%DE = (D_1 - D_2) \ / \ D_2 \times 100$$

Where "D_1" and "D_2" respectively exhibit the total and un-incorporated drug concentration.

4.1.1.1. Transmission electron microscopy (TEM). RLX-PNPs were subjected to morphological analysis via TEM (TEM, Hitachi Japan). Before the analysis, sample was prepared for TEM study. Briefly, few drops the final formulation of RLX-PNPs was diluted with deionized water and were kept on a copper grid coated with carbon film. The sample was dried for 10 s followed by negative staining with 1% phosphotungstic acid and air drying. The prepared sample was scanned with TEM at accelerated voltage of 100 kV [29].

4.2. Fourier-transform infrared spectroscopy (FTIR)

In order to check the possible exchange of functional groups among the components of RLX-PNPs, FTIR (Thermo Scientific, USA) analysis was performed. Fleetingly, each sample (5 mg) was compacted along with 200 mg of KBr into a disc with the help of hydraulic press. Each sample was scanned at the wavelength range from 400 to 4000 cm^{-1} and the FTIR spectra was recorded [30]. OMINIC™ spectra software was used in order to check and document the spectra [31].

4.2.1. Differential scanning calorimeter (DSC)

Thermal behavior of the RLX-PNPs and its constituents including pure RLX, CTX and physical mixture were executed using DSC (Q200 New Castle, USA). Prior to that, the samples were lyophilized by means of a freeze dryer (SP Scientific, UK). Momentarily, 5 mg of each sample was weighted in aluminum pan, followed by shielding with aluminum lid. Each sample was analyzed using DSC in the temperature range of 50–300 °C. Temperature of the system was set to rise at a constant rate of 10 °C/min [32,33]. System was cooled down before each analysis.

4.3. Powder X-rays diffractometery (PXRD)

Crystallinity of the pure RLX, CTX, physical mixture and RLX-PNPs was determined using powder X-ray diffractometers (Rigaku, Japan). Briefly, all the samples were exposed to XRD scans in the range of 5–50° 2 theta. The scans were accomplished on a Ni-filtered Cu target such that the theta range was increased at 1°/sec. The current and voltage of the system was kept as 100 mA and 100 kV,

respectively [34,35].

4.4. In-vitro drug release characterization and kinetic models evaluation

In-vitro release performance of the RLX-PNPs was investigated using dialysis bag method. Analysis was performed at simulated physiological pH conditions of pH 7.4 which was prepared using phosphate buffer [36]. Dissolution assembly (DT-820, ERWEKA, Germany) was used for this study. Small sections (3–4 cm) of dialysis bag (MWCO 12–14 kDa) were cut and tied on one end, followed by addition of 10 mg of equivalent quantity of RLX using RLX-Suspension and RLX-PNPs from the other end of dialysis bag and were clipped tightly. These bags were submerged in respective dissolution assemblies holding 500 ml of the dissolution medium. Temperature of the system was set at 36.5 ± 0.5 °C and the paddles were set to rotate at 70 rpm. At pre-selected time periods, 3 ml sample was withdrawn from each container followed by a replacement with equal quantity of dissolution medium. Suitable dilutions of the samples were prepared and analyzed using HPLC as discussed above for the quantification of RLX and the release graphs were drawn using Sigma plot software. Additionally, DD-Solver was used to check the best fitted release model [37,38].

4.5. Accelerated stability studies

Stability studies of the optimized RLX-PNPs were performed at accelerated stability conditions including refrigerating temperature and above physiological temperature for a period of 6 months [39,40]. Fleetingly, freshly prepared optimized RLX-PNPs were prepared, taken in 8 different glass vials and 4 each were stored at their respective temperatures in stability chamber at 4 ± 2 °C and 40 ± 2 °C [41]. Prior to their storage, samples were subjected to physicochemical characterizations including particle size, PDI, zeta potential, %DE and physical stability. At predetermined time periods (month, 1, 2, 4, and 6), one of the samples from each group were taken and subjected to stability evaluation on the above mentioned parameters [36,42].

4.6. Preclinical studies

Sprague-Dawley rats with 240 ± 5 g weights and 11–12 weeks age were used as experimental animals in this study. Animal were treated as per the guidelines for animal studies by the national institute of health (NIH) and ARRIVE guidelines for the use of laboratory animals. All the animal safety procedures were approved from the bioethical committee of Quaid-i-Azam University, Islamabad, Pakistan under the approval number FBS-2022-0156 and medical ethics committee, Henan province hospital under the approval number PZ-Hnszv-2022-026. Animals were feed with standard laboratory food and were allowed easy access to tap water before and during the experimentation. Temperature of the animal house was set at 23 ± 2 °C and humidity was controlled at 56 ± 5% during the animal studies.

4.7. Pharmacokinetics study

4.7.1. Administration and blood collection

Pharmacokinetic profiles of the RLX-PNPs and RLX-Suspension were determined using Sprague-Dawley rats in order to check the bioavailability of RLX [43,44]. Twelve rats were equally divided into 2 groups. To one group, RLX-Suspension was administered, while the other group received RLX-PNPs at corresponding dose of 5 mg/kg. Rats were anaesthetized with isoflurane and their individual weights were recorded. They were positioned on a dissection on their back, with knotted arms and legs using a thread. Hair form their right leg were shaved and femoral artery was opened to insert a polyethylene tube was inserted to obtain blood samples at desired time intervals. Both the tests groups were orally administered with the respective RLX-Suspension and RLX-PNPs by means of stomach sonde needle. At specified time intermissions (30 min, 50 min, 1h, 2, 3, 4, 6, 12, and 24 h), 280–300 μl blood was withdrawn from the cannulated femoral artery. The samples were taken in pre-heparinized Eppendorf tubes followed by their centrifugation in order to isolate the blood plasma. The plasma was temporarily stored at −80 °C. At a suitable time, quantification of the RLX in plasma was performed using HPLC as discussed above [11].

4.8. Blood treatment and data generation

After the completion of animal testing, the stored blood plasma was taken out from refrigerator and thawed at room temperature. Plasma (150 μl) was mixed with acetonitrile (155 μl), which had 10 μl naproxen (internal standard) dissolved in it. The mixture was centrifuged at 13,000 rpm for 10 min to remove proteins. After centrifugation, the supernatant (20 μl) was quantified via HPLC for RLX concentration [45]. Pharmacokinetic profiles of both the testing groups were plotted using Sigma plot software. Moreover, pharmacokinetic parameters were determined using WinNonlin software (Version 5.2; Pharsight, Mountain View, USA). Among them, maximum concentration (C_{max}), area under the curve (AUC) $_{0\sim infinity}$, maximum time (t_{max}), elimination constant (K_{el}), and half-life ($t_{1/2}$) were determined and tabulated [1,33].

4.9. Induction and treatment of OP

Ovariectomy surgery was done to induce OP in Sprague-Dawley rats. Twenty four rats were equally allocated in four groups. One groups was considered as normal group, without ovariectomy surgery and thus not treated with any formulation. Surgery of the other

03 groups were done in order to develop ovariectomy model [46]. After 11 weeks of the surgery, rats were distributed in three groups [47,48]. One group was orally given 1.4 mg/kg RLX-PNPs, whereas the 2nd group received 5.6 mg/kg RLX suspension orally. However, the 3rd group didn't receive any formulation and was considered untreated control. The treatment continued for 28 days. The data obtained was used in the generation of graphs after biochemical analysis.

5. Biochemical investigations

5.1. Serum biomarkers

At day 29, the rats serum was collected from the retro-orbital sinus. Prior to it, the rats were anaesthetized with isoflurane and the obtained blood was stored in sterilized tubes. The blood samples were kept at room temperature for 15 min and were allowed to coagulate, followed by their centrifugation at 9000 rpm for 10 min in order to separate serum from the blood. Temperature of the centrifuge machine was set at 3 °C. Serum was kept at −80 °C until used for the quantification of biomarkers. At a suitable time, the serum biomarkers counting alkaline phosphatase (ALP) and calcium (Ca), were evaluated by means of ELISA testing [49].

5.2. Urine biomarkers

Urine biomarkers are usually accessed to check the bone growth status in experimental models. Here, pyridinoline (Pyr) and deoxypyridinoline (DPyr) levels were investigated which explicitly are used as bone resorption markers. Method comparisons were carried out on RLX-PNPs and RLX-Suspension after OP treatment. Urine samples from all the tests groups were collected after 12h fasting into sterile containers, enfolded in aluminum foils and stored at −20 °C. They were subjected to Pyr and DPyr quantification as reported earlier [50–52].

5.3. Statistical analysis

Various statistical tolls and software's were used in this study including, student *t*-test and One-way ANOVA test. At ($p < 0.05$), data was considered significantly different. Bio render software, DD solver and sigma plot (Version 12) were utilized for the data generation, analysis, graphical presentation and images creation. Data was analyzed in either mean ± SD ($n = 3$ or $n = 6$).

6. Results

6.1. Optimization of RLX-PNPs

RLX-PNPs were optimized via trial and error method. Briefly, the specified quantities of raloxifene (RLX), chitosan (CTX), sodium tripolyphosphate (STPP), and Tween®80 were used in the preparation of different formulations, which were characterized to determine the most suitable formulation. Variables set for these experiments included particle size, zeta potential and percent drug entrapment (%DE). Results of these experiments are given in Table 1.

In the first phase of optimization study, amount of CTX was optimized by changing its concentration in the range of 10–25 mg, whereas, the concentration of other ingredients of the PNPs system were kept constant (Table 1, F-1 to F-4). Results showed that the particle size and %DE was significantly increased from 89.8 nm to 237.6 nm and 67.21%–78.14%, respectively, with the increase in concentration of CTX. It was also evident that the %DE was increased with surge in concentration of CTX, however after some added concentration, the change become insignificant. The increased concentration of CTX has also displayed a significant effect on the zeta potential of all the prepared formulations. PDI was observed in the range of 0.141–0.296 and zeta potential was noted in range of

Table 1
Optimization of the raloxifene-loaded polymeric nanoparticles (RLX-PNPs).

Code	CTX (mg)	STPP (mg)	RLX (mg)	Tween 80 (mg)	Particle size (nm)	PDI	Zeta Potential (mV)	%DE
F1	10	4	5	2	89.8 ± 1.8	0.171 ± 0.008	+22.3 ± 0.7	67.21 ± 0.94
F-2	15	4	5	2	114.3 ± 1.2	0.162 ± 0.008	+25.4 ± 1.1	73.10 ± 0.65
F-3	20	4	5	2	178.7 ± 2.9	0.201 ± 0.014	+28.3 ± 0.4	75.14 ± 1.16
F-4	25	4	5	2	237.6 ± 4.2	0.296 ± 0.015	+32.5 ± 0.2	78.14 ± 2.10
F-5	15	2	5	2	108.8 ± 1.3	0.153 ± 0.008	+26.7 ± 1.1	69.01 ± 0.63
F-6	15	6	5	2	127.2 ± 1.4	0.172 ± 0.008	+23.8 ± 0.3	80.17 ± 1.15
F-7	15	8	5	2	159.7 ± 1.1	0.161 ± 0.013	+21.9 ± 0.6	82.22 ± 1.79
F-8	15	10	5	2	204.4 ± 3.5	0.153 ± 0.005	+19.4 ± 0.3	74.11 ± 1.54
F-9	15	6	3	2	121.3 ± 1.1	0.177 ± 0.007	+25.7 ± 1.6	76.94 ± 1.55
F-10	15	6	7	2	136.1 ± 0.7	0.164 ± 0.008	+24.8 ± 1.0	87.91 ± 0.49
F-11	15	6	10	2	142.7 ± 1.1	0.170 ± 0.011	+25.3 ± 1.6	88.67 ± 0.64
F-12	15	6	10	3	134.5 ± 1.3	0.196 ± 0.006	+24.4 ± 0.1	91.73 ± 0.77
F-13	15	6	7	5	146.3 ± 1.4	0.155 ± 0.009	+24.5 ± 0.6	84.41 ± 1.15

Here, CTX represents chitosan, STPP shows Sodium tripolyphosphate, RLX represents raloxifene, PDI represents polydispersity index and %DE represents percent drug entrapment. Means ± SD ($n = 3$).

+19.4 to +32.5 mV for all the formulations. Formulation having 15 mg of CTX (F-2) was considered suitable for further optimization process due to its low particle size, PDI, adequate zeta potential and better drug entrapment.

In the second phase of the study, the quantity of STPP was optimized by varying its concentration from 2 to 10 mg (Table 1, F-2 and F5–F8). The concentration of RLX and Tween®80 was kept constant. An increase in particle size was observed with increased concentration of STPP (108.8 nm–204.4 nm). Similarly, an initial increase in the %DE of PNPs was observed with increased concentration of STPP (2–8 mg), however, the entrapment was decreased upon adding more concentration of STPP (10 mg). The amount of STPP didn't change the values on PDI meaningfully. However, with increased STPP concentration the zeta potential was significantly decreased from +26.7 to +19.4 mV. Among the tested formulations, F-6 was selected for further studies based on its suitable particle properties and drug entrapment.

In the third phase of study, the concentration of RLX was optimized by preparing different formulations having RLX quantity in the range of 3–10 mg, whereas the concentration of Tween®80 was kept constant and the concentrations of CTX and STPP were already optimized (Table 1, F6, F9–F11). Results showed that increased concentration of RLX has increased the particle size in the range of 121.3 nm–131.4 nm. Likewise, %DE was meaningfully enhanced from 76.94% to 91.73% as the concentration of RLX was increased. After the third phase of optimization, F-11 was carried forward as the optimized formulation, based on its particle properties (particle size, PDI and zeta potential) and the highest %DE encountered. In the final phase of optimization study, concentration of Tween®80 was optimized by changing its quantity in the range of 2–5 mg as reported in Table 1, F11 and F12–F13. A meaningfully reduced particle size (142.7–131.4 nm) and increased %DE (88.67–91.73%) was noted as the concentration of Tween® 80 was changed from 2 to 3 mg. However, upon further increase in concentration of Tween®80 (F-13), the particle size was enlarged again (146.3 nm) and the %DE was reduced to 84.41%. These results demonstrated that the constituents of the RLX-PNPs have significant effect of the particle properties, mainly on particle size and %DE. Based on these findings, F-12 was chosen as the most appropriate formulation with 134.5 ± 1.3 nm size, 0.196 ± 0.006 PDI, zeta potential of +24.4 ± 1.2 mV, and 91.73 ± 0.77% %DE of RLX (Fig. 2AB, Table 1).

6.2. TEM analysis

The morphology of the RLX-PNPs was analyzed using TEM and the reports are displayed in Fig. 3. As shown in TEM micrograph, the RLX-PNPs have spherical shaped particles with distinct boundaries and uniform distribution. Particle analysis displayed well segregation and particle sizes below 200 nm. These results were in accordance with the Zetasizer results which showed nano sized particle formation with low PDI and stable preparation.

6.3. FTIR analysis

FTIR analysis of the RLX-PNPs and its components including RLX, CTX, STPP and physical mixture is reported in Fig. 4. As can be seen, no major chemical interactions were found among the ingredients of RLX-PNPs and their corresponding peaks were preserved in PNPs and physical mixture. The principal peaks of RLX were found in 1590–1600 $cm^{-1}$and 1640-1660 cm^{-1} region, respectively presenting the presence of (–C–O–C–) stretching and (C═O stretching). The representative peaks of CTX were present at 1000-1100 cm^{-1} region, representing the presence of C═O. Similarly, the corresponding peak of NH_2 in CTX was found at 1650-1700 cm^{-1} region. In the case of STPP, the representative FTIR peak of PO_4 was detected at 1127 cm^{-1}. The physical mixture and RLX-PNPs demonstrated the presence of all the corresponding peaks of constituents mainly at 900, 1100, 1600 and 1660 region of the FTIR, indicating their chemical compatibility.

6.3.1. Differential scanning calorimetry (DSC)

DSC study of the RLX-PNPs was performed in order to check the thermal behavior of the formulation and its comparison with its

Fig. 2. Particle characterization of the RLX-PNPs. (A) Particle size, (B) Zeta potential.

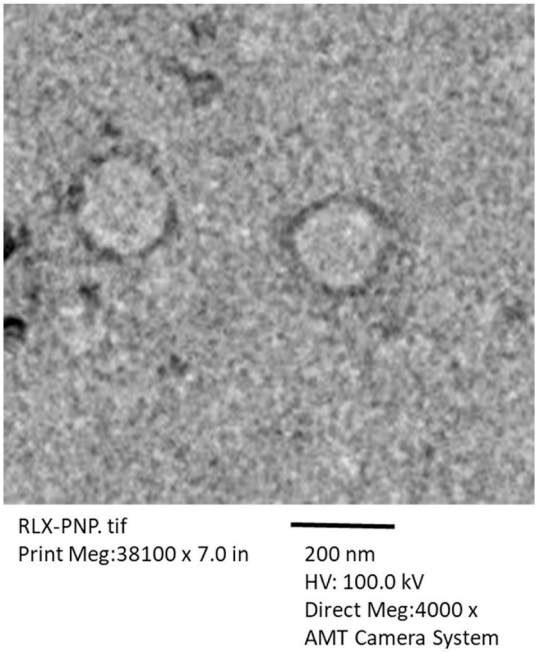

Fig. 3. Transmittance Electron Microscopy (TEM) analysis of the RLX-PNPs (4,000X).

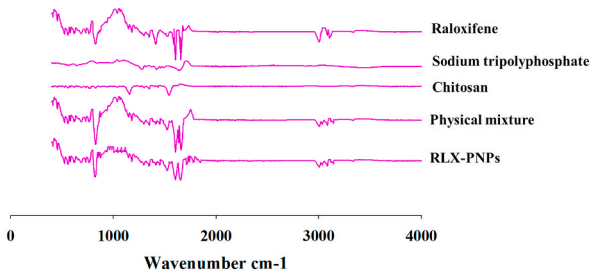

Fig. 4. Fourier Transform Infrared Spectrophotometry (FTIR) spectra of Raloxifene, C Chitosan, STPP, their physical mixture and RLX-PNPs.

individual ingredients, including RLX, CTX and their physical mixture. The DSC thermograms are reported in Fig. 5. As indicated, a sharp endothermic peak at 266 °C was observed for pure RLX, indicating its melting point [52,53]. The CTX showed its corresponding endothermic peak at 105 °C due to loss of water content [54]. Similarly, physical mixture exhibited the corresponding peaks of both RLX and CTX indicating that the heating phase of a mixture is the apex of its fundamental ingredients [55]. The DSC thermogram of

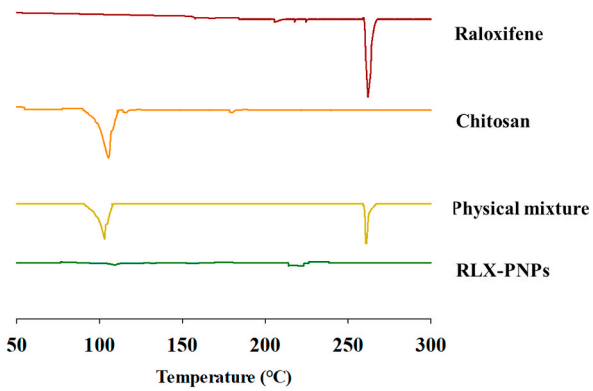

Fig. 5. Dynamic scattering Calorimetry (DSC) of Raloxifene, Chitosan, their physical mixture and RLX-PNPs.

RLX-PNPs showed no corresponding peaks of drug and polymers, indicating the thermal stability of the formulation and the conversion of crystalline drug and polymer to amorphous form.

6.4. Powder X-ray diffractometer (PXRD)

Crystallinity of the RLX-PNPs and its constituents were investigated in PXRD analysis and the results are displayed in Fig. 6. Outcomes of this study revealed that the pure drug and CTX have crystalline structures which were also exhibited in their physical mixture. However, the final formulation demonstrated the conversion of crystalline constituents into amorphous form, as their corresponding peaks were absent. Briefly, pure RLX showed its distinguished PXRD peaks to 2θ ranges of 15.11°, 17.13°, 11.22°, 23.31°, and 24.17, signifying its crystalline nature. Similarly, the PXRD peaks of CTX were observed at 2θ range of 10.12°, and 20.26° demonstrating its crystalline nature. Physical mixture showed all the principal peaks of RLX and CTX, indicating the presence of crystallinity of both the ingredients. However, when processed during the formation of PNPs, the crystalline PXRD peaks of both the ingredients were vanished. Mainly, the crystalline drug was converted into amorphous form [56,57].

6.5. In-vitro drug release and kinetic models

The in-vitro drug release profile of RLX was accomplished at pH 7.4 and was compared with RLX-Suspension. As indicated in Fig. 7, RLX-Suspension released about 42% of the RAL in 1 h followed by entire drug release in 3.5 h. However, RLX-PNPs released a total of 10% RLX in 1 h and sustained the drug release for about 24 h, by releasing around 90% of the incorporated drug. These results demonstrated a comparatively quick release from the RLX-Suspension. Whereas, the RLX-PNPs showed a meaningfully retarded drug release, which could be attributed to the sustained release effect of the polymer. Analysis of various kinetic models revealed the highest R^2value (0.998) for Korsmeyer-Peppas, proving its suitability for RLX release from RLX-PNPs. The value of "n" was found to be 0.598 showing the release to be non-fickian diffusion.

6.6. Stability studies

Results of the accelerated stability analysis of the RLX-PNPs are presented in Table 2. As stated earlier, this study was performed at 4 ± 2 °C and 40 ± 2 °C temperatures for a period of 6 months. No significant changes on the particle size, PDI, %DE and zeta potential were observed at both the temperatures for 4 months. Although a small variation in all the parameters observed, yet the formulation remind physically stable and the change was non-significant. Results further showed that after 6 months, the formulation stored at 4 ± 2 °C remained stable, demonstrating within range particle properties and %DE. However, formulation stored at 40 ± 2 °C showed a significant increase in particle size (131.4–209.3 nm) and meaningful decrease (91.73–81.31%) in %DE after six months. Thus, it is evident that the RLX-PNPs may be stored at refrigerating and accelerating conditions for 4 months, however, it should be placed at refrigerator if long term stability is required.

7. In-vivo studies

7.1. Pharmacokinetic study

Pharmacokinetic studies of RLX-PNPs were performed in rats to check the bioavailability of RLX. The results are demonstrated in Fig. 8 and Table 3. As indicated, meaningfully improved bioavailability of RLX was exhibited by the PNPs, when compared with RLX-suspension. Briefly, a significantly different C_{max}(7.38 ± 0.49 μg/ml) and AUC (2092.83 ± 53.64 μg h/ml) of RLX was observed after oral administration of RLX-PNPs as compared to the C_{max}(1.02 ± 0.18 μg/ml) and AUC (263.81 ± 19.95 μg*h/ml) of the RLX-suspension. Similarly, T_{max} of RLX-PNPs was found (3.39 ± 0.12 h), whereas the T_{max} of RLX-Suspension was noted as (2.68 ± 0.11 h). Moreover, other parameters namely half-life ($t_{½}$) and elimination constant ($K_{el}h^{-1}$) didn't change significantly. The comparison of plasma drug concentrations between RLX-Suspension and RLX-PNPs is displayed in Fig. 8.

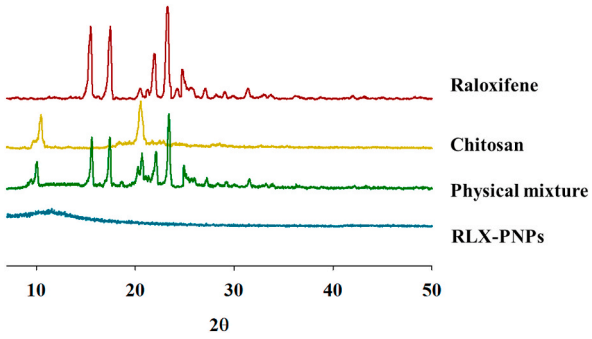

Fig. 6. Powder X-rays Diffractometer (PXRD of Raloxifene, Chitosan, their physical mixture and RLX-PNPs.

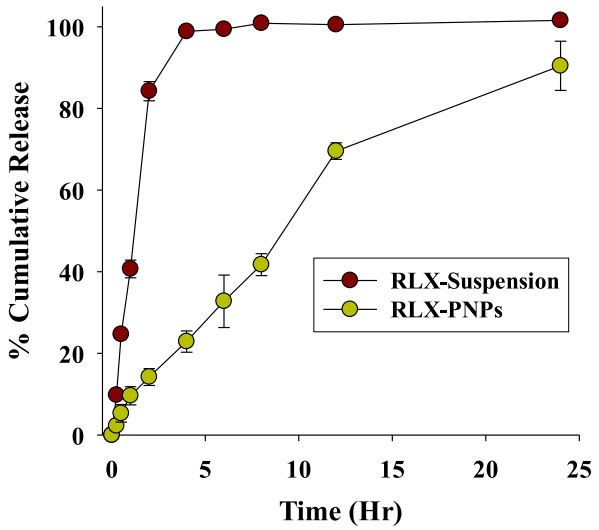

Fig. 7. In-vitro cumulative release profiles of RLX-PNPs and RLX-Suspension. Mean ± SD (n = 3).

Table 2
Stability study of RLX-PNPs at different storage temperatures.

Month	At temperature 4 ± 2 °C					At temperature 40 ± 2 °C				
	Particle Size(nm)	PDI	Zeta Potential (mV)	%DE	Physical stability	Particle Size(nm)	PDI	Zeta Potential (mV)	%DE	Physical stability
0	131.4 ± 1.3	0.141 ± 0.006	+26.4 ± 0.1	91.73 ± 0.77	+++	131.4 ± 1.3	0.141 ± 0.006	+26.4 ± 0.1	91.73 ± 0.77	+++
1	133.1 ± 1.4	0.155 ± 0.007	+26.3 ± 1.5	91.62 ± 2.64	+++	134.5 ± 2.7	0.145 ± 0.008	+26.9 ± 1.2	91.92 ± 2.74	+++
2	137.5 ± 4.3	0.177 ± 0.013	+25.9 ± 1.6	90.72 ± 4.11	+++	142.8 ± 6.4	0.185 ± 0.024	+26.8 ± 1.8	89.20 ± 3.92	+++
4	143.8 ± 7.5	0.192 ± 0.008	+25.5 ± 2.5	90.66 ± 4.19	+++	150.4 ± 10.5	0.214 ± 0.013	+23.8 ± 0.9	87.04 ± 5.10	++
6	148.5 ± 5.6	0.208 ± 0.010	+25.2 ± 2.6	89.11 ± 5.02	+++	209.3 ± 11.2	0.356 ± 0.007	+20.1 ± 1.3	81.31 ± 1.52	——

Here, PDI represents Polydispersity Index and %DE: Percent Drug Entrapment. Mean ± standard deviation (n = 3).

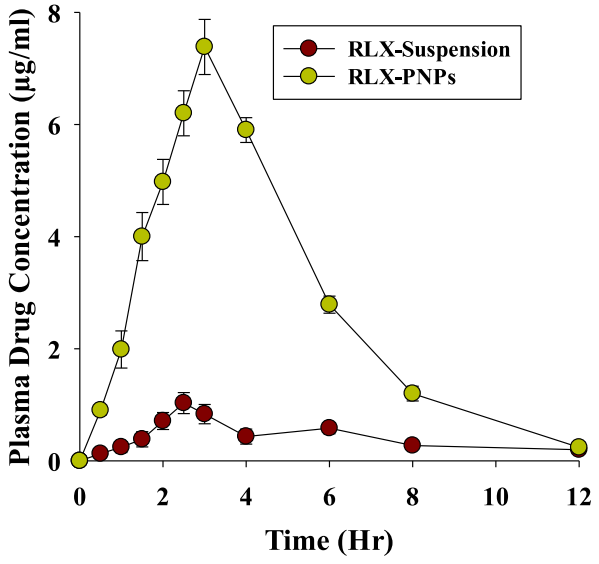

Fig. 8. Plasma drug concentration time profiles of RLX-PNPs and RLX-Suspension. Data was analyzed in sextuplicate (n = 6).

Table 3
Pharmacokinetic study of RLX-PNPs and RLX-suspension in Sprague-Dawley rats.

Pharmacokinetic Parameters	RLX-PNPs	RLX-Suspension
AUC (μg*h/ml)	2092.83 ± 53.64*	263.81 ± 19.95
T_{max} (h)	3.39 ± 0.12*	2.68 ± 0.11
C_{max} (μg/ml)	7.38 ± 0.49*	1.02 ± 0.18
$t_{½}$ (h)	7.32 ± 0.73	7.15 ± 0.55
$K_{el}(h^{-1})$	5.49 ± 0.51	4.77 ± 0.42

Each value represents the mean ± S.D. (n = 6). *P < 0.05 compared to RLX-Suspension.

7.2. Biochemical analysis

Biochemical analyses of various biomarkers were investigated in OP induced animals after oral treatment using the RLX-PNPs and RLX-Suspension as reported in Figs. 9 and 10. Briefly, serum quantification of alkaline phosphatase and calcium and urine levels of pyridinoline (Pyr) and deoxypyridinoline (DPyr) were determined and compared with normal control and OP induced un-treated control groups.

7.3. Alkaline phosphatase

Serum biochemical tests revealed significantly amplified levels of ALP in OP induced untreated control group (489.13 ± 22.14 u/l) and RLX-Suspension treated group (403.20 ± 18.76 u/l). However, RLX-PNPs treated groups displayed evocatively abridged ALP levels (327.87 ± 14.78u/l), just like the normal control (315.65 ± 13.54u/l). Statistically, high ALP values were exhibited by the untreated and RLX-Suspension treated groups showed less efficacy of the Suspension when compared with the RLX-PNPs. Moreover, the RLX-PNPs showed significantly reduced level of ALP, indicating its improved anti osteoporotic effect.

7.4. Calcium level

Results of the calcium study showed significantly greater levels of calcium in the OP induced untreated control and RLX-Suspension treated groups. Momentarily, their serum calcium levels were noted as 8.01 ± 0.68 mg/dL and 5.87 ± 0.56 mg/dL, respectively (Fig. 9B). However, RLX-PNPs treated group expressively abridged the serum calcium level (3.79 ± 0.23 mg/dL) as observed in normal control group (3.65 ± 0.17 mg/dL). These results were suggestive of the reduced bone disease in RLX-PNPs group when associated with the corresponding groups.

7.5. Pyridinoline (Pyr) level

To further assess the bone growth status the urinary Pyr and DPyr levels were also investigated (Fig. 10). Both Pyr and DPyr are specific bone resorption markers. Results showed a meaningfully increased level of Pyr in the animal groups sequentially as OP induced untreated group 37.4 ± 2.3 nM/Mm followed by RLX-Suspension 33.3 ± 1.9 nM/Mm (Fig. 10A). Contrary to that, a significantly reduced level of Pyr (24.2 ± 1.6 nM/Mm) was observed in animal group treated with RLX-PNPs. This value were as low as observed in normal control group (23.1 ± 1.5 nM/Mm), indicating that the PNPs have the capability to treat OP.

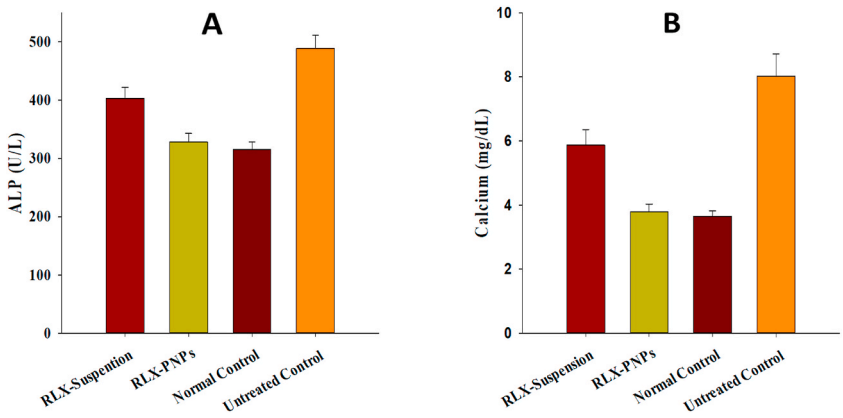

Fig. 9. Assessment of the serum biochemical markers level, (A) Alkaline phosphatase; (B) Calcium, in osteoporosis induced Sprague-Dawley rats after treatment with RLX-Suspension, RLX-PNPs and untreated control groups and its comparison with normal control group. Mean ± SD (n = 3).

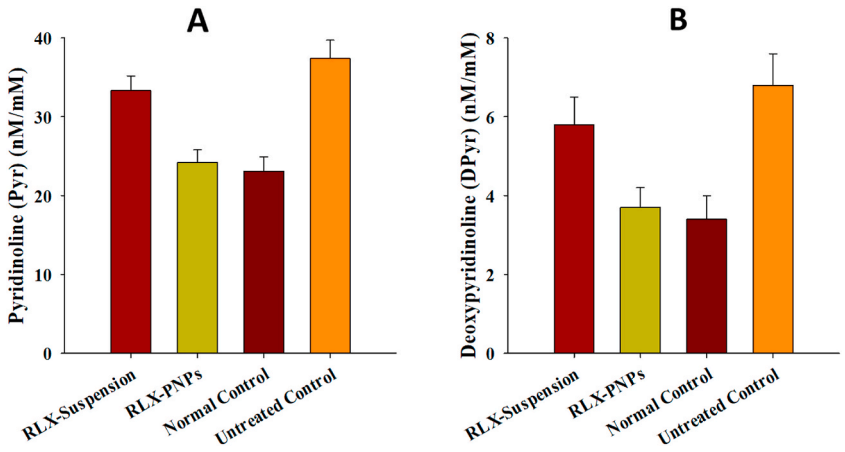

Fig. 10. Assessment of the urine biochemical markers level, (A) Pyridinolin; (B) DeoxyPyridinol in osteoporosis induced Sprague-Dawley rats after treatment with RLX-Suspension, RLX-PNPs and untreated control groups and its comparison with normal control group. Mean ± SD (n = 3).

7.6. Deoxypyridinoline (DPyr) level

The results of DPyr level are reported in (Fig. 10B). As can be seen, the level of DPyr was respectively observed as 6.8 ± 0.8 nM/Mm and 5.8 ± 0.8 nM/Mm for OP induced untreated and RLX-Suspension. Moreover, this level was meaningfully reduced in RLX-PNPs treated group which showed 3.7 ± 0.4 nM/Mm and normal control groups (3.4 ± 0.4 nM/Mm), respectively. This data showed the efficacy of PNPs in reducing the OP conditions in rats.

8. Discussion

Polymeric nanoparticles (PNPs) are versatile nano-system which have recently get applause for the targeted delivery, improved pharmaceutical and pharmacological effect of the incorporated drugs and safety profile due to use of biodegradable polymers [23,58,59]. Some of the major compensations of PNPs includes, their ability to control the drug release, guard the incorporated drugs against the microenvironment of disease and human complex system, enhancing the bioavailability and therapeutic index of drugs [60,61]. Various methods are used for the preparation of PNPs, selection of which is mostly dependent on the selected drug, rout of administration and required therapeutic effects. These methods include, ionic gelation method, solvent evaporation, emulsification, reverse salting out and nano precipitation [24,25,62]. Among them ionic gelation method is one of the most suitable technique owing to its easy operation, affordability and reproducibility [63]. CTX was selected as a polymer owing to its excellent capability of drug entrapment, biodegradation and biocompatibility [64]. STPP was selected based on its suitable cross linking abilities. Moreover tween 80 was used as a surfactant. Concentrations of all the ingredients of the polymeric nanoparticles were optimized in a series of experiments.

Significantly increased particle size and drug entrapment was observed with amplified concentration of CTX. This could be because of the formation of highly viscous CTX solution obtained as a result of high CTX concentration [65]. Moreover, the significantly upsurge %DE of RLX could be attributed to the capability of formation of ionic gel of CTX's and inhibition of drug movement to peripheral phase. Additionally, the increased concentration of CTX showed increased zeta potential owing to its cationic nature. Moreover, the presence of protonated amine groups in CTX also contribute to it [66]. However, the PDI was not significantly changed. Likewise, the particle size was increased significantly with increased concentration of STPP. This could be because of the amplified rigidity of CTX and STPP cross linkages. Moreover, increased concentration of tripolyphosphoric ions leads to their improved cross-linking with CTX that ultimately results in the formation of denser shells [67]. Besides, the increased STPP concentration initially increased the %DE of RLX significantly, however above certain concentration, the %DE was meaningfully decreased. Conversely, increased quantity of STPP showed meaningfully decreased zeta potential. It could be because of the better gradation of gelation between phosphate of STPP and nitrogen of CTX [68]. Whereas, the PDI was not meaningfully changed. Increased concentration of RLX did not have a substantial effect on the particle size, PDI, zeta potential and %DE of the RLX-PNPs. Finally, the increased concentration of Tween 80 has initially reduced the particle size, however, above certain concentration the partial size was found significantly. Unlikely, the %DE was meaningfully increased initially and then decreased with the increase in surfactant concentration.

TEM analysis of the RLX-PNPs showed well segregated particles with clear boundaries, rounded shapes and a mean diameter of 200 nm. The particles were found uniformly distributed with low PDI index indicating stable RLX-PNPs. Moreover, FTIR spectra exhibited no chemical interactions among the ingredients of the PNPs. Similarly, the corresponding peaks of all the ingredients were found well-preserved in their physical mixture and RLX-PNPs. Exact peaks in particular FTIR region revealed the occurrence for amide-I of CTX [69]. DSC analysis was performed to check the thermal behavior of the PNPs and its components compared with physical mixture. The transition temperature of the ingredients of formulation doesn't differ when combined with other constituents of the formulation. Moreover, the physical mixture of these constituents may results in comparatively less thermal endotherms owing to the diminished

purity of the ingredients [70]. DSC analysis showed that the RLX, CTX exhibited their respective thermograms individually as well as when assorted together in physical mixture. However, when incorporated in PNPs, the representative endothermal peaks of all the ingredients vanishes indicating the formation of stable nanoparticles and the conversion of crystalline drug into amorphous drug [71] Various other studies have reported similar results, when the drug was incorporated in nanoparticle drug delivery systems [72]. Furthermore, the change observed in the temperature denotes the conversion of crystalline nature of drug to amorphous [73]. Additionally, the PXRD analysis was executed to check the crystallinity of the drug and its physical mixture compared with the RLX-PNPs. Most of the pure drugs exist in crystalline form, which significantly reduce the solubility and bioavailability of the drugs [74]. Results demonstrated the crystalline nature of pure RLX and endothermic peaks of CTX when observed for crystallinity study. Similar peaks were noted in the physical mixture of drugs and polymer. However, all the corresponding peaks were absent in the RLX-PNPs indicating the conversion of crystalline drug to amorphous form. Moreover, it was hypothesized that the solubilization and bioavailability of the drug would be enhanced.

This hypothesis was further tested in in-vitro release assay. It is worth mention that drug release and the pattern of drug release form a nano system is important to produce the desired therapeutic effect, which is associated with the drug solubilization and release from the system [75,76]. Moreover, it ensure the availability of drug at desired concentration at a specific period of time [77,78]. As desired, a meaningfully controlled release of the RLX was observed from PNPs owing to the polymer effect on drug release. Moreover, based on the increased R^2 values, it was observed that the drug release from polymeric system follow the Korsmeyer-Peppas model. Similar reports are reported earlier in literature [79]. Furthermore, the "n" values of RLX-PNPs determined that the formulation followed atypical non-fickian diffusion for releasing drug. It has already been reported that CTX nanoparticles showed this sort of behavior [80].

Stability studies of the RLX-PNPs formulation designated no meaningful difference ($P > 0.05$) in the particle size and PDI of formulation at each point time for a period of 6 months at 4 °C, showing the stability of formulation at refrigerating temperature. However, formulation remained stable at 40 °C for 4 months only and at 6 months the particle size was significantly enhanced. This could be because of the accelerated temperature conditions which may results in destabilizing the formulation. Overall, these results advocated on the stability of the RLX-PNPs for 6 months at 4 °C, and for 4 months at 40 °C.

The outcomes of pharmacokinetics data reported in this study demonstrated that PNPs is an exceptional nano system, particularly for drugs with poor solubility to show enhanced bioavailability and improved therapeutic effects [1,81]. An evocatively upgraded bioavailability of the RLX was observed by the RLX-PNPs when associated with RLX suspension. This incredible augmentation RLX bioavailability could be attributed to the formation of nano size polymeric particles, better dissolution and solubilization effect [81, 82].

Various biochemical markers via serum and urine were performed to check the effectiveness of the developed formulation in OP. It has been reported earlier that ALP and calcium serum levels are increased in bone disease [46]. In this study, increased ALP and calcium values were observed in untreated OP induced and RLX-Suspension treated rats groups indicating the porosity of bones and accompanying bone disease. These results indicated that immediate treatment should be provided to individuals suffering from OP, to avoid bones damage over the extended period of time. Unlike them, RLX-PNPs treated groups exhibited profoundly abridged ALP and calcium levels. Their values were not meaningfully different than the normal control group. Moreover, this study stated that RLX-PNPs have recovered the compromised bones both by delaying bone resorption and improving bone formation.

Urine biochemical markers including pyridinoline (Pyr) and deoxypyridinoline (DPyr) were investigated in OP induced rats and were associated with RLX-PNPs and RLX-Suspension treated and normal groups. These Pyr and DPyr associated fibrils have a prominent role in covalently bonding the collagen molecules in bone matrix. More importantly, the DPyr marker is more precise for bone. Moreover, variation in their levels leads to bone metabolism, escalating childhood, menopause, osteo-malacia, hyperparathyroidism and hyperthyroidism, and dropping due to estrogen and bisphosphonate treatment. This study exhibited significantly reduced levels of Pyr and DPyr in RLX-PNPs, which were more like the levels observed in normal group. However, meaningfully enhanced levels of both the markers were observed in RLX-Suspension and untreated groups. Overall it was established that the RLX-PNPs have the capability to treat the bone disease, especially the OP and help improve the bone growth.

9. Conclusion

This study concluded the formation of polymeric nanoparticles of raloxifene having particles in nano size range with suitable drug entrapment. Particles characterization demonstrated the formation of positively charged spherical and uniform particles. The solid state characterization showed the conversion of crystalline drug to amorphous form. Moreover, the functional groups of all the ingredients were intact without any major shifts. RLX-PNPs exhibited a meaningfully sustained release and significantly enhanced bioavailability of the RLX when compared with RLX-Suspension. Additionally, the RLX-PNPs exhibited a significantly improved anti osteoporotic effect in OP induced Sprague-Dawley rats model. Most importantly the meaningfully reduced levels of serum ALP and calcium and urine Pyr and DPyr showed the augmented potential of RLX towards OP treatment.

Author contribution statement

Zhonghua Gou: Conceived and designed the experiments; Performed the experiments. </p>;
Rabia Afza: Muhammad Moneeb: Performed the experiments. </p>
Saif Ullah Khan: Zakir Ali: Analyzed and interpreted the data. </p>
Muhammad Waseem Khan: Contributed reagents, materials, analysis tools or data; Wrote the paper. </p>

Sibgha Batool: Contributed reagents, materials, analysis tools or data. </p>
Fakhar Ud Din: Conceived and designed the experiments; Wrote the paper. </p>

Data availability statement

Data will be made available on request.

Funding

The research work was funded by HEC through its grant No:20-14604/NRPU/R&D/HEC/2021. Also, funding was provided by Henan Province Traditional Chinese Medicine Top Talents Training Project (Yuwei Chinese Medicine Letter [2021] No. 15).

Declaration of competing interest

The authors declare that they have no known competing financial interests or personal relationships that could have appeared to influence the work reported in this paper.

Acknowledgment

The authors acknowledge Higher Education Commission (HEC) Pakistan for funding this study.

References

[1] G. Yu, Z. Ali, A.S. Khan, K. Ullah, H. Jamshaid, A. Zeb, M. Imran, S. Sarwar, H.-G. Choi, F. ud Din, Preparation, pharmacokinetics, and antitumor potential of miltefosine-loaded nanostructured lipid carriers, Int. J. Nanomed. 16 (2021) 3255, https://doi.org/10.1016/j.carbpol.2016.06.096.
[2] D. Kendler, J.-J. Body, M. Brandi, R. Broady, J. Cannata-Andia, M. Cannata-Ortiz, A. El Maghraoui, G. Guglielmi, P. Hadji, D. Pierroz, Osteoporosis management in hematologic stem cell transplant recipients: executive summary, J. Bone Oncol. 28 (2021), 100361, https://doi.org/10.1016/j.jbo.2021.100361.
[3] S. Gyanewali, P. Kesharwani, A. Sheikh, F.J. Ahmad, R. Trivedi, S. Talegaonkar, Formulation development and in vitro–in vivo assessment of protransfersomal gel of anti-resorptive drug in osteoporosis treatment, Int. J. Pharm. 608 (2021), 121060, https://doi.org/10.1016/j.ijpharm.2021.121060.
[4] J.Y. Reginster, N. Burlet, Osteoporosis: a still increasing prevalence, Bone 38 (2) (2006) 4–9, https://doi.org/10.1016/j.bone.2005.11.024.
[5] D.K. Dhanwal, E.M. Dennison, N.C. Harvey, C. Cooper, Epidemiology of hip fracture: worldwide geographic variation, IJO 45 (1) (2011) 15–22, https://doi.org/10.4103/0019-5413.73656.
[6] M.T. Drake, B.L. Clarke, E.M. Lewiecki, The pathophysiology and treatment of osteoporosis, Clin. Ther. 37 (8) (2015) 1837–1850, https://doi.org/10.1016/j.clinthera.2015.06.006.
[7] Y. Cai, T. Gao, S. Fu, P. Sun, Development of zoledronic acid functionalized hydroxyapatite loaded polymeric nanoparticles for the treatment of osteoporosis, Exp. Ther. Med. 16 (2) (2018) 704–710, https://doi.org/10.3892/etm.2018.6263.
[8] M.N. Shekhawat, Z. Surti, N. Surti, Biodegradable in situ gel for subcutaneous administration of simvastatin for osteoporosis, Indian J. Pharm. Sci. 80 (2) (2018) 395–399, https://doi.org/10.4172/pharmaceutical-sciences.1000371.
[9] G. Pizzino, N. Irrera, F. Galfo, G. Oteri, M. Atteritano, G. Pallio, F. Mannino, A. D'Amore, E. Pellegrino, F. Aliquò, Adenosine receptor stimulation improves glucocorticoid-induced osteoporosis in a rat model, Front. Pharmacol. 8 (2017) 558, https://doi.org/10.3389/fphar.2017.00558.
[10] J. Štěpán, J. Rosa, K. Pavelka, Raloxifen–nevyužitá možnost prevence a léčby postmenopauzální osteoporózy, Vnitr. Lek. 62 (10) (2016) 781–788.
[11] M.C. Fontana, A. Beckenkamp, A. Buffon, R.C.R. Beck, Controlled release of raloxifene by nanoencapsulation: effect on in vitro antiproliferative activity of human breast cancer cells, Int. J. Nanomed. 9 (2014) 2979, https://doi.org/10.2147/IJN.S62857.
[12] A.A. Date, M.D. Joshi, V.B. Patravale, Parasitic diseases: liposomes and polymeric nanoparticles versus lipid nanoparticles, Adv. Drug Deliv. Rev. 59 (6) (2007) 505–521, https://doi.org/10.1016/j.addr.2007.04.009.
[13] J. Kreuter, Liposomes and nanoparticles as vehicles for antibiotics, Infection 19 (4) (1991) S224–S228, https://doi.org/10.1007/BF01644038.
[14] C.P. Reis, R.J. Neufeld, A.J. Ribeiro, F. Veiga, I. Nanoencapsulation, Methods for preparation of drug-loaded polymeric nanoparticles, Nanomed. Nanotechnol. Biol. Med. 2 (1) (2006) 8–21, https://doi.org/10.1016/j.nano.2005.12.003.
[15] R. Gul, N. Ahmed, N. Ullah, M.I. Khan, A. Elaissari, A.u. Rehman, Biodegradable ingredient-based emulgel loaded with ketoprofen nanoparticles, AAPS PharmSciTech 19 (2018) 1869–1881, https://doi.org/10.1208/s12249-018-0997-0.
[16] M.B. Subudhi, A. Jain, A. Jain, P. Hurkat, S. Shilpi, A. Gulbake, S.K. Jain, Eudragit S100 coated citrus pectin nanoparticles for colon targeting of 5-fluorouracil, Materials 8 (3) (2015) 832–849, https://doi.org/10.3390/ma8030832.
[17] Min-Soo Kim, I.-h. Baek, Fabrication and evaluation of valsartan–polymer–surfactant composite nanoparticles by using the supercritical antisolvent process, Int. J. Nanomed. 9 (2014) 5167, https://doi.org/10.2147/IJN.S71891.
[18] C.J. Bowerman, J.D. Byrne, K.S. Chu, A.N. Schorzman, A.W. Keeler, C.A. Sherwood, J.L. Perry, J.C. Luft, D.B. Darr, A.M. Deal, Docetaxel-loaded PLGA nanoparticles improve efficacy in taxane-resistant triple-negative breast cancer, Nano Lett. 17 (1) (2017) 242–248, https://doi.org/10.1021/acs.nanolett.6b03971.
[19] J. Movellan, P. Urban, E. Moles, J.M. de la Fuente, T. Sierra, J.L. Serrano, X. Fernandez-Busquets, Amphiphilic dendritic derivatives as nanocarriers for the targeted delivery of antimalarial drugs, Biomaterials 35 (27) (2014) 7940–7950, https://doi.org/10.1016/j.biomaterials.2014.05.061.
[20] K.V. Jardim, G.A. Joanitti, R.B. Azevedo, A.L. Parize, Physico-chemical characterization and cytotoxicity evaluation of curcumin loaded in chitosan/chondroitin sulfate nanoparticles, Mater. Sci. Eng. C 56 (2015) 294–304, https://doi.org/10.1016/j.msec.2015.06.036.
[21] M. Rinaudo, Chitin and chitosan: properties and applications, Prog. Polym. Sci. 31 (7) (2006) 603–632, https://doi.org/10.1016/j.progpolymsci.2006.06.001.
[22] A. Bernkop-Schnurch, S. Dunnhaupt, Chitosan-based drug delivery systems, Eur. J. Pharm. Biopharm. 81 (3) (2012) 463–469, https://doi.org/10.1016/j.ejpb.2012.04.007.
[23] M.M. Khan, S.S. Zaidi, F.J. Siyal, S.U. Khan, G. Ishrat, S. Batool, O. Mustapha, S. Khan, F. ud Din, Statistical optimization of co-loaded rifampicin and pentamidine polymeric nanoparticles for the treatment of cutaneous leishmaniasis, J. Drug Deliv. Sci. Technol. 79 (2023), 104005, https://doi.org/10.1016/j.jddst.2022.104005.
[24] P. Calvo, C. Remunan Lopez, J.L. Vila Jato, M. Alonso, Novel hydrophilic chitosan polyethylene oxide nanoparticles as protein carriers, J. Appl. Polym. Sci. 63 (1) (1997) 125–132, https://doi.org/10.1002/(SICI)1097-4628(19970103)63, 1< 125::AID-APP13>3E3.0.CO;2-4.
[25] N. Rajendran, R. Natrajan, S. Kumar, S. Selvaraj, Acyclovir-loaded chitosan nanoparticles for ocular delivery, Asian J. Pharm. 4 (4) (2010), https://doi.org/10.4103/0973-8398.76749.

[26] F. ud Din, O. Mustapha, D.W. Kim, R. Rashid, J.H. Park, J.Y. Choi, S.K. Ku, C.S. Yong, J.O. Kim, H.-G. Choi, Novel dual-reverse thermosensitive solid lipid nanoparticle-loaded hydrogel for rectal administration of flurbiprofen with improved bioavailability and reduced initial burst effect, Eur. J. Pharm. Biopharm. 94 (2015) 64–72, https://doi.org/10.1016/j.ejpb.2015.04.019.

[27] F. ud Din, D.W. Kim, J.Y. Choi, R.K. Thapa, O. Mustapha, D.S. Kim, Y.-K. Oh, S.K. Ku, Y.S. Youn, K.T.J.A.b. Oh, Irinotecan-loaded double-reversible thermogel with improved antitumor efficacy without initial burst effect and toxicity for intramuscular administration, Acta Biomater. 54 (2017) 239–248, https://doi.org/10.1016/j.actbio.2017.03.007.

[28] K. Shahzad, S. Mushtaq, M. Rizwan, W. Khalid, M. Atif, F.U. Din, N. Ahmad, R. Abbasi, Z.J.M.S. Ali, E. C, Field-controlled magnetoelectric core-shell CoFe2O4@BaTiO3 nanoparticles as effective drug carriers and drug release in vitro, Mater. Sci. Eng. C. 119 (2021), 111444, https://doi.org/10.1016/j.msec.2020.111444.

[29] A.U. Khan, H. Jamshaid, F. ud Din, A. Zeb, G.M. Khan, Designing, optimization and characterization of Trifluralin transfersomal gel to passively target cutaneous leishmaniasis, J. Pharm. Sci (2022) 1798–1811, https://doi.org/10.1016/j.xphs.2022.01.010.

[30] M. Bibi, F. ud Din, Y. Anwar, N.A. Alkenani, A.T. Zari, M. Mukhtiar, I.M.A. Zeid, E.H. Althubaiti, H. Nazish, A. Zeb, Cilostazol-loaded solid lipid nanoparticles: bioavailability and safety evaluation in an animal model, J. Drug Deliv. Sci. Technol. 74 (2022), 103581, https://doi.org/10.1016/j.jddst.2022.103581.

[31] S. Rabia, N. Khaleeq, S. Batool, M.J. Dar, D.W. Kim, F.-U. Din, G.M. Khan, Rifampicin-loaded nanotransferosomal gel for treatment of cutaneous leishmaniasis: passive targeting via topical route, Nanomedicine 15 (2) (2020) 183–203, https://doi.org/10.2217/nnm-2019-0320.

[32] Namrah Khan, F.A. Shah, I. Rana, M.M. Ansari, F. ud Din, S.Z.H. Rizvi, W. Aman, G.-Y. Lee, E.-S. Lee, Nanostructured lipid carriers-mediated brain delivery of carbamazepine for improved in vivo anticonvulsant and anxiolytic activity, Int. J. Pharm. 577 (2020), 119033, https://doi.org/10.1016/j.ijpharm.2020.119033.

[33] J. Suk Kim, F. ud Din, S.M. Lee, D.S. Kim, M.R. Woo, S. Cheon, S.H. Ji, J.O. Kim, Y.S. Youn, Comparison of three different aqueous microenvironments for enhancing oral bioavailability of sildenafil: solid self-nanoemulsifying drug delivery system, amorphous microspheres and crystalline microspheres, Int. J. Nanomed. 16 (2021) 5797. https://doi/full/10.2147/IJN.S324206.

[34] Jung Suk Kim, J.H. Park, S.C. Jeong, D.S. Kim, A.M. Yousaf, F.U. Din, J.O. Kim, C.S. Yong, Y.S. Youn, Novel revaprazan-loaded gelatin microsphere with enhanced drug solubility and oral bioavailability, J. Microencapsul. 35 (5) (2018) 421–427, https://doi.org/10.1080/02652048.2018.1515997.

[35] R. Rashid, D.W. Kim, A.M. Yousaf, O. Mustapha, F. ud Din, J.H. Park, C.S. Yong, Y.-K. Oh, Y.S. Youn, J.O. Kim, Comparative study on solid self-nanoemulsifying drug delivery and solid dispersion system for enhanced solubility and bioavailability of ezetimibe, Int. J. Nanomed. 10 (2015) 6147. https://doi/full/10.2147/IJN.S91216.

[36] A.S. Khan, F. ud Din, Z. Ali, M. Bibi, F. Zahid, A. Zeb, G.M. Khan, Development, in vitro and in vivo evaluation of miltefosine loaded nanostructured lipid carriers for the treatment of Cutaneous Leishmaniasis, Int. J. Pharm. 593 (2021), 120109, https://doi.org/10.1016/j.ijpharm.2020.120109.

[37] Husna Khalid, S. Batool, F.u. Din, S. Khan, G.M. Khan, Macrophage targeting of nitazoxanide-loaded transethosomal gel in cutaneous leishmaniasis, R. Soc. Open Sci. 9 (10) (2022), 220428, https://doi.org/10.1098/rsos.220428.

[38] F.U. Din Dar, G.M. Khan, Sodium stibogluconate loaded nano-deformable liposomes for topical treatment of leishmaniasis: macrophage as a target cell, Drug Deliv. 25 (1) (2018) 1595–1606, https://doi.org/10.1080/10717544.2018.1494222.

[39] D. Kalaria, G. Sharma, V. Beniwal, M. Ravi Kumar, Design of biodegradable nanoparticles for oral delivery of doxorubicin: in vivo pharmacokinetics and toxicity studies in rats, Pharm. Res. (N. Y.) 26 (3) (2009) 492–501, https://doi.org/10.1007/s11095-008-9763-4.

[40] S. Jain, A. Mittal, A. K Jain, R. R Mahajan, D. Singh, Cyclosporin A loaded PLGA nanoparticle: preparation, optimization, in-vitro characterization and stability studies, Curr. Nanosci. 6 (4) (2010) 422–431, https://doi.org/10.2174/157341310791658937.

[41] A. Anjum, K. Shabbir, F.U. Din, S. Shafique, S.S. Zaidi, A.H. Almari, T. Alqahtani, A. Maryiam, M. Moneeb Khan, A. Al Fatease, Co-delivery of amphotericin B and pentamidine loaded niosomal gel for the treatment of Cutaneous leishmaniasis, Drug Deliv. 30 (1) (2023), 2173335, https://doi.org/10.1080/10717544.2023.2173335.

[42] A.K. Jain, N.K. Swarnakar, C. Godugu, R.P. Singh, S. Jain, The effect of the oral administration of polymeric nanoparticles on the efficacy and toxicity of tamoxifen, Biomaterials 32 (2) (2011) 503–515, https://doi.org/10.1016/j.biomaterials.2010.09.037.

[43] O. Mustapha, F.U. Din, D.W. Kim, J.H. Park, K.B. Woo, S.-J. Lim, Y.S. Youn, K.H. Cho, R. Rashid, A.M. Yousaf, Novel piroxicam-loaded nanospheres generated by the electrospraying technique: physicochemical characterisation and oral bioavailability evaluation, J. Microencapsul. 33 (4) (2016) 323–330, https://doi.org/10.1080/02652048.2016.1185475.

[44] J.H. Park, J.H. Cho, D.S. Kim, J.S. Kim, F.U. Din, J.O. Kim, C.S. Yong, Y.S. Youn, K.T. Oh, D.W. Kim, Revaprazan-loaded surface-modified solid dispersion: physicochemical characterization and in vivo evaluation, Pharm. Dev. Technol. 24 (6) (2019) 788–793, https://doi.org/10.1080/10837450.2019.1597114.

[45] S. Maqsood, F.U. Din, S.U. Khan, E. Elahi, Z. Ali, H. Jamshaid, A. Zeb, T. Nadeem, W. Ahmed, S. Khan, Levosulpiride-loaded nanostructured lipid carriers for brain delivery with antipsychotic and antidepressant effects, Life Sci. 311 (2022), 121198, https://doi.org/10.1016/j.lfs.2022.121198.

[46] D.N. Kalu, The ovariectomized rat model of postmenopausal bone loss, J. Bone Miner. Res. 15 (3) (1991) 175–191, https://doi.org/10.1016/0169-6009(91)90124-I.

[47] F. Zakir, A. Ahmad, M.A. Mirza, K. Kohli, F.J. Ahmad, Exploration of a transdermal nanoemulgel as an alternative therapy for postmenopausal osteoporosis, J. Drug Deliv. Sci. Technol. 65 (2021), 102745, https://doi.org/10.1016/j.jddst.2021.102745.

[48] N. Yousefzadeh, K. Kashfi, S. Jeddi, A. Ghasemi, Ovariectomized rat model of osteoporosis: a practical guide, EXCLI J 19 (2020) 89, https://doi.org/10.17179/excli2019-1990.

[49] F. Zakir, A. Ahmad, U. Farooq, M.A. Mirza, A. Tripathi, D. Singh, F. Shakeel, S. Mohapatra, F.J. Ahmad, K. Kohli, Design and development of a commercially viable in situ nanoemulgel for the treatment of postmenopausal osteoporosis, Nanomedicine 15 (12) (2020) 1167–1187, https://doi.org/10.2217/nnm-2020-0079.

[50] S.P. Robins, H. Woitge, R. Hesley, J. Ju, S. Seyedin, M.J. Seibel, Direct, enzyme-linked immunoassay for urinary deoxypyridinoline as a specific marker for measuring bone resorption, J. Bone Miner. Res. 9 (10) (1994) 1643–1649, https://doi.org/10.1002/jbmr.5650091019.

[51] T. Miazgowski, S. Czekalski, A 2-year follow-up study on bone mineral density and markers of bone turnover in patients with long-standing insulin-dependent diabetes mellitus, Osteoporos. Int. 8 (5) (1998) 399–403, https://doi.org/10.1007/s001980050082.

[52] B.M. El-Houssieny, E.Z. El-Dein, H.M. El-Messiry, Enhancement of solubility of dexibuprofen applying mixed hydrotropic solubilization technique, Drug Discov. Ther. 8 (4) (2014) 178–184, https://doi.org/10.5582/ddt.2014.01019.

[53] Q. Khalid, M. Ahmad, M.U. Minhas, Synthesis of β-cyclodextrin hydrogel nanoparticles for improving the solubility of dexibuprofen: characterization and toxicity evaluation, Drug Dev. Ind. Pharm. 43 (11) (2017) 1873–1884, https://doi.org/10.1080/03639045.2017.1350703.

[54] S. Das, W.K. Ng, P. Kanaujia, S. Kim, R.B. Tan, Formulation design, preparation and physicochemical characterizations of solid lipid nanoparticles containing a hydrophobic drug: effects of process variables, Colloids Surf., B 88 (1) (2011) 483–489, https://doi.org/10.1016/j.colsurfb.2011.07.036.

[55] Y. Choi, K.A. Min, C.-K. Kim, Development and evaluation of dexibuprofen formulation with fast onset and prolonged effect, Drug Dev. Ind. Pharm. 45 (6) (2019) 895–904, https://doi.org/10.1080/03639045.2019.1576720.

[56] D.S. Kim, D.W. Kim, K.S. Kim, J.S. Choi, Y.G. Seo, Y.S. Youn, K.T. Oh, C.S. Yong, J.O. Kim, S.G. Jin, Development of a novel l-sulpiride-loaded quaternary microcapsule: effect of TPGS as an absorption enhancer on physicochemical characterization and oral bioavailability, Colloids Surf., B 147 (2016) 250–257, https://doi.org/10.1016/j.colsurfb.2016.08.010.

[57] D.S. Kim, J.S. Choi, D.W. Kim, K.S. Kim, Y.G. Seo, K.H. Cho, J.O. Kim, C.S. Yong, Y.S. Youn, S.-J. Lim, Comparison of solvent wetted and kneaded l-sulpiride loaded solid dispersions: powder characterization and in vivo evaluation, Int. J. Pharm. 511 (1) (2016) 351–358, https://doi.org/10.1016/j.ijpharm.2016.07.006.

[58] A. Cano, M. Ettcheto, J.-H. Chang, E. Barroso, M. Espina, B.A. Kühne, M. Barenys, C. Auladell, J. Folch, E.B. Souto, Dual-drug loaded nanoparticles of Epigallocatechin-3-gallate (EGCG)/Ascorbic acid enhance therapeutic efficacy of EGCG in a APPswe/PS1dE9 Alzheimer's disease mice model, J. Contr. Release 301 (2019) 62–75, https://doi.org/10.1016/j.jconrel.2019.03.010.

[59] A. Cano, E. Sánchez-López, M. Ettcheto, A. López-Machado, M. Espina, E.B. Souto, R. Galindo, A. Camins, M.L. García, P. Turowski, Current advances in the development of novel polymeric nanoparticles for the treatment of neurodegenerative diseases, Nanomedicine 15 (12) (2020) 1239–1261, https://doi.org/10.2217/nnm-2019-0443.
[60] K.S. Soppimath, T.M. Aminabhavi, A.R. Kulkarni, W.E. Rudzinski, Biodegradable polymeric nanoparticles as drug delivery devices, J. Contr. Release 70 (1–2) (2001) 1–20, https://doi.org/10.1016/S0168-3659(00)00339-4.
[61] D.E. Owens III, N.A. Peppas, Opsonization, biodistribution, and pharmacokinetics of polymeric nanoparticles, Int. J. Pharm. 307 (1) (2006) 93–102, https://doi.org/10.1016/j.ijpharm.2005.10.010.
[62] A. Zielińska, F. Carreiró, A.M. Oliveira, A. Neves, B. Pires, D.N. Venkatesh, A. Durazzo, M. Lucarini, P. Eder, A.M. Silva, Polymeric nanoparticles: production, characterization, toxicology and ecotoxicology, Molecules 25 (16) (2020) 3731, https://doi.org/10.3390/molecules25163731.
[63] M.J. Masarudin, S.M. Cutts, B.J. Evison, D.R. Phillips, P.J. Pigram, Factors determining the stability, size distribution, and cellular accumulation of small, monodisperse chitosan nanoparticles as candidate vectors for anticancer drug delivery: application to the passive encapsulation of [14C]-doxorubicin, Nanotechnol. Sci. Appl. 8 (2015) 67. https://doi/full/10.2147/NSA.S91785.
[64] M.A. Ghaz Jahanian, F. Abbaspour Aghdam, N. Anarjan, A. Berenjian, H. Jafarizadeh Malmiri, Application of chitosan-based nanocarriers in tumor-targeted drug delivery, Mol. Biotechnol. 57 (3) (2015) 201–218, https://doi.org/10.1007/s12033-014-9816-3.
[65] B.K. Patel, R.H. Parikh, P.S. Aboti, Development of oral sustained release rifampicin loaded chitosan nanoparticles by design of experiment, J. Drug Deliv. 2013 (2013) 1–10, https://doi.org/10.1155/2013/370938.
[66] R. Al-Kassas, J. Wen, A.E.-M. Cheng, A.M.-J. Kim, S.S.M. Liu, J. Yu, Transdermal delivery of propranolol hydrochloride through chitosan nanoparticles dispersed in mucoadhesive gel, Carbohydr, Polym 153 (2016) 176–186, https://doi.org/10.1016/j.carbpol.2016.06.096.
[67] B. Gajra, R.R. Patel, C. Dalwadi, Formulation, optimization and characterization of cationic polymeric nanoparticles of mast cell stabilizing agent using the Box–Behnken experimental design, Drug Dev. Ind. Pharm. 42 (5) (2016) 747–757, https://doi.org/10.3109/03639045.2015.1093496.
[68] M.A. Mahmood, A. Madni, M. Rehman, M.A. Rahim, A. Jabar, Ionically cross-linked chitosan nanoparticles for sustained delivery of docetaxel: fabrication, post-formulation and acute oral toxicity evaluation, Int. J. Nanomed. 14 (2019), 10035. https://doi/full/10.2147/IJN.S232350.
[69] A. Madni, P.M. Kashif, I. Nazir, N. Tahir, M. Rehman, M.I. Khan, M.A. Rahim, A. Jabar, Drug-polymer interaction studies of cytarabine loaded chitosan nanoparticles, J. Chem. Soc. Pak. 39 (6) (2017).
[70] S. Botha, A. Lötter, Compatibility study between atenolol and tablet excipients using differential scanning calorimetry, Drug Dev. Ind. Pharm. 16 (12) (1990) 1945–1954, https://doi.org/10.3109/03639049009028349.
[71] F. ud Din, A. Zeb, K.U. Shah, Development, in-vitro and in-vivo evaluation of ezetimibe-loaded solid lipid nanoparticles and their comparison with marketed product, J. Drug Deliv. Sci. Technol. 51 (2019) 583–590, https://doi.org/10.1016/j.jddst.2019.02.026.
[72] B. Imran, F. ud Din, Z. Ali, A. Fatima, M.W. Khan, D.W. Kim, M. Malik, S. Sohail, S. Batool, M. Jawad, Statistically designed dexibuprofen loaded solid lipid nanoparticles for enhanced oral bioavailability, J. Drug Deliv. Sci. Technol. 77 (2022), 103904, https://doi.org/10.1016/j.jddst.2022.103904.
[73] J.L. Ford, A.F. Stewart, J.-L. Dubois, The properties of solid dispersions of indomethacin or phenylbutazone in polyethylene glycol, Int. J. Pharm. 28 (1) (1986) 11–22, https://doi.org/10.1016/0378-5173(86)90142-0.
[74] R. Tiwari, G. Tiwari, B. Srivastava, A.K. Rai, Solid dispersions: an overview to modify bioavailability of poorly water soluble drugs, Int. J. Pharmtech Res. 1 (4) (2009) 1338–1349.
[75] S. Batool, S. Sohail, F. ud Din, A.H. Alamri, A.S. Alqahtani, M.A. Alshahrani, M.A. Alshehri, H.G. Choi, A detailed insight of the tumor targeting using nanocarrier drug delivery system, Drug Deliv. 30 (1) (2023), 2183815, https://doi.org/10.1080/10717544.2023.2183815.
[76] A. Khan, B. Shal, A.U. Khan, K.U. Shah, S.S. Zahra, I. ul Haq, F. ud Din, H. Ali, S. Khan, Neuroprotective mechanism of Ajugarin-I against Vincristine-Induced neuropathic pain via regulation of Nrf2/NF-κB and Bcl2 signalling, Int. Immunopharm. 118 (2023), 110046, https://doi.org/10.1016/j.intimp.2023.110046.
[77] S. Gelperina, K. Kisich, M.D. Iseman, L. Heifets, The potential advantages of nanoparticle drug delivery systems in chemotherapy of tuberculosis, Am. J. Respir. Crit. Care Med. 172 (12) (2005) 1487–1490, https://doi.org/10.1164/rccm.200504-613PP.
[78] Y.H. Bae, K. Park, Targeted drug delivery to tumors: myths, reality and possibility, J. Contr. Release 153 (3) (2011) 198, https://doi.org/10.1016/j.jconrel.2011.06.001.
[79] Farahani Gooneh, S.M. Sahar Naghib, M.R. Naimi Jamal, A novel and inexpensive method based on modified ionic gelation for pH-responsive controlled drug release of homogeneously distributed chitosan nanoparticles with a high encapsulation efficiency, Fibers Polym. 21 (9) (2020) 1917–1926, https://doi.org/10.1007/s12221-020-1095-y.
[80] N. Gulati, U. Nagaich, S.A. Saraf, Intranasal delivery of chitosan nanoparticles for migraine therapy, Sci. Pharm. 81 (3) (2013) 843–854, https://doi.org/10.3797/scipharm.1208-18.
[81] u. Din, W. Fakhar, Aman I Ullah, O.S. Qureshi, O. Mustapha, S. Shafique, A.J.I.j.o.n. Zeb, Effective use of nanocarriers as drug delivery systems for the treatment of selected tumors, Int. J. Nanomed. 12 (2017) 7291. https://doi/full/10.2147/IJN.S146315.
[82] F. Sabir, M.I. Asad, M. Qindeel, I. Afzal, M.J. Dar, K.U. Shah, A. Zeb, G.M. Khan, N. Ahmed, F.U. Din, Polymeric nanogels as versatile nanoplatforms for biomedical applications, J. Nanomater. 2019 (2019) 1–16, https://doi.org/10.1155/2019/1526186.